Low-field magnetotransport study of localization in a mesoscopic antidot array

Y. Chen, R. J. Nicholas, and G. M. Sundaram
Physics Department, Clarendon Laboratory, Oxford University, Parks Road, Oxford OX1 3PU, United Kingdom

P. J. Heard
Oxford Instruments, Eynsham, United Kingdom

P. D. Prewett
Rutherford and Appleton Laboratory, Chilton, Didcot, United Kingdom

J. E. F. Frost and G. A. C. Jones
Cavendish Laboratory, Madingley Road, Cambridge CB3 0EH, United Kingdom

D. C. Peacock
Cavendish Laboratory, Madingley Road, Cambridge CB3 0EH, United Kingdom
and GEC Hirst Research Center, East Lane, Wembley HA9 7PP, United Kingdom

D. A. Ritchie
Cavendish Laboratory, Madingley Road, Cambridge CB3 0EH, United Kingdom
(Received 2 June 1992)

Low-field negative magnetoresistance has been studied on G_a^+ ion focused-ion-beam-patterned GaAs/$Ga_{1-x}Al_xAs$ heterojunctions as a function of carrier density and temperature. The negative magnetoresistance (NMR) is very large at low densities and decreases with increasing carrier density, giving a magnetoconductance linear in T at low densities but closer to a $\ln T$ dependence at higher values. The NMR of this grid structure is well explained using weak localization modified by boundary scattering in an array of one-dimensional point contacts. The NMR disappears after illumination as the patterning is screened by the increased electron density. From this model, we fit the phase-breaking rate as $1/\tau_\phi = A + BT$, where the constant term is attributed to boundary scattering and the linear temperature dependence arises from electron-electron scattering.

I. INTRODUCTION

A strong negative magnetoresistance (NMR) is a characterization feature in two-dimensional (2D) arrays of antidots fabricated by focused-ion-beam (FIB) techniques.[1,2] This paper reports a detailed study of this phenomenon, and relates this to the nature of the localization and conduction processes. A large number of works have recently studied the properties of 2D dot (or antidot) lattices[3,4] usually fabricated on GaAs/$Ga_{1-x}Al_xAs$ heterojunctions; however, the large negative magnetoresistance seems to be a particular feature of the very strong modulating potential produced by FIB patterning. A study of the temperature and magnetic-field dependences allows us to fit the properties in terms of a largely 1D conduction process limited by the weak interconnections between the antidot regions.

The samples were produced as described in paper I,[1] by a process of FIB patterning onto conventional GaAs/$Ga_{1-x}Al_xAs$ heterojunctions that had high mobilities of $\mu = 0.65(1.2) \times 10^6$ cm^2/Vs at $n = 3.5(4.5) \times 10^{11}$ cm^{-2} in the dark (fully illuminated) before patterning. The sample details are given in Table I. According to the damage-induced depletion theory,[5] a space-charge region is formed around each implanted spot, characterized by a depletion length,[2] leading to a region of exclusion for electrons. Between the two nearest spots, a saddle-shaped potential constricts the electron flow and a reservoir forms away from the damaged regions, thus acting as an antidot. In Table I, the width W_n and the length l_n of the constrictions is given, as deduced in Sec. IV. The pattern configurations of the samples are as described in paper I.[1] The magnetotransport measurements used conventional ac lock-in technique at ~ 15 Hz, at currents of ~ 50 nA, taking care to avoid possible electron heating effects. Temperatures were measured using a calibrated Ge resistor, and the carrier densities were varied using persistent photoexcitation with a red LED, and leaving the system to equilibrate for a period of hours before measurement.[6]

II. RESULTS

A. Results at 4.2 K

The negative magnetoresistance in low fields was observed in all of the samples except sample 2, which was the most weakly patterned. Figure 1 presents a variety of magnetoresistance traces as a function of B recorded on sample 1 at 4.2 K after varying bursts of light by LED.

TABLE I. The pattern parameters for the four samples that have the same sample numbers as those in paper I (Ref. 1). Because no NMR was found on the most weakly patterned sample 2, the values of W_n and l_n for this sample in the table are absent.

Samples	Configuration size (μm)	Separation of spot (μm)	Accelerating energy (keV)	Spot size (μm)	W_n (nm)	l_n (nm)
1	100×250	1.0	20	0.4	57.6	340
2	100×250	2.0	10	0.8		
3	100×400	0.8	20	0.4	67.4	328
4	100×400	1.0	20	0.4	69.8	374

The carrier density labeled on each trace corresponds to that in the constrictions, which was measured from the Shubnikov–de Haas (SdH) oscillations in higher fields.[1] For a particular trace, with the magnetic field increasing from zero, the magnetoresistance first decreases, giving a negative magnetoresistance, and then the SdH oscillations emerge above ~0.5 T, the precise value depending on the concentration. In sufficiently high fields, the SdH oscillations become dominant as edge states propagate through the constrictions. The NMR, which can be as big as 13.6 kΩ per square, with a relative change of $\Delta\rho_{xx}(B)/\rho_{xx}(0)$ of 46% at 1.03×10^{11} cm^{-2} (nearly dark)

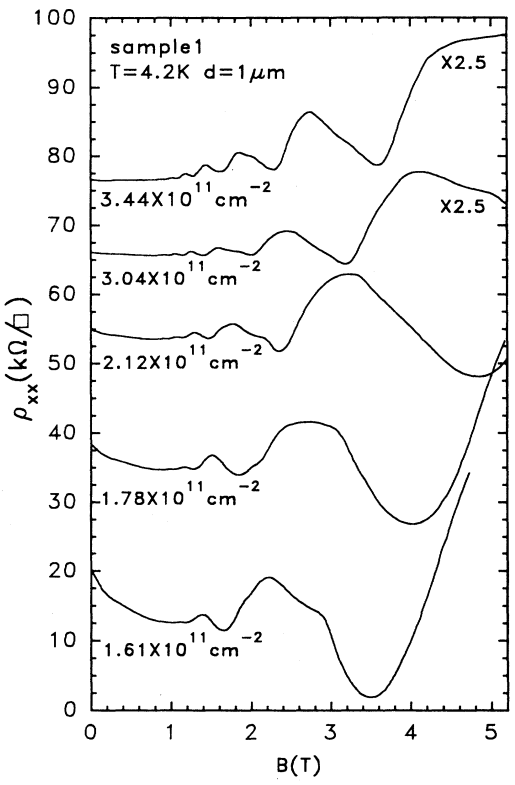

FIG. 1. Magnetoresistance traces taken at five fixed carrier densities at 4.2 K. The traces with concentrations above 1.61×10^{11} cm^{-2} are offset for clarity. Please refer to paper I (Ref. 1) for detailed pattern configurations of samples. The carrier densities labeled on the traces are those measured by SdH oscillations in strong fields.

is a strong function of the carrier density. For higher densities, the NMR almost completely disappears, suggesting that the NMR (or the localization) in our samples stems from the pattern-induced depletion potentials instead of random impurity potentials as in disordered systems.[7] The electrons were shown in paper I to strongly screen the patterning potential, so that the modulating potential profile falls as the carrier density (and Fermi energy E_F) rises. This is associated with a rapid rise in conductivity as the constrictions open up. We therefore associate the large NMR with the presence of the applied patterning potential. With increasing concentration, the field range in which the delocalization occurs falls from ~1.4 to 0.5 T or less. For comparison with theory we use the magnetoconductance $G(B)$ (the inverse of R_{xx}), which is shown as a function of B in Fig. 2 for one sample for various carrier densities. A comparison of the carrier-density dependence of the conductance for two different pattern periods is shown in Fig. 3.

B. Temperature dependence

Temperature dependence of the NMR was studied from 4.2–0.6 K, and Fig. 4 shows a typical plot of the low-field magnetoconductance for a set of temperatures in a strongly patterned structure. The solid lines are fits that will be described below. The low-field region is used for study here to avoid any influence of the Shubnikov–de Haas oscillations.

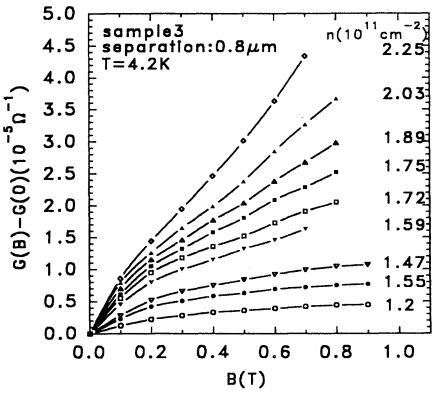

FIG. 2. The increase in magnetoconductance $G(B)-G(0)$ measured on sample 3 at 4.2 K for several different electron densities. The solid lines are a guide for the eye.

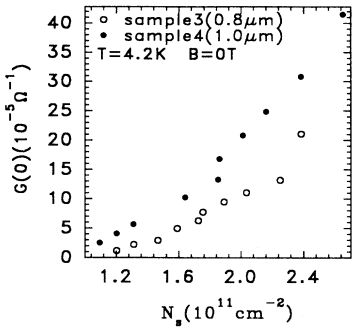

FIG. 3. Conductance at 4.2 K as a function of carrier density in samples 3 and 4.

All samples show a conductivity that decreases as temperature falls, but this is strongly related to the strength of the patterning and carrier density. Figure 5 shows a typical example for a 1-μm-period structure. For the two lowest densities 1.03 and 1.27×10^{11} cm^{-2} there is quite a large linear increase in conductivity with temperature, but for the higher densities this begins to saturate and is much closer to a $\ln T$ dependence. For example, when the conductance at 2.0×10^{11} cm^{-2} is replotted as a function of $\ln T$ as presented in the uppermost curve of Fig. 5, it shows a good straight line. Similar detailed studies were done on several samples at typically four or five different densities.

III. ANALYSIS

It is well known that NMR is explained in disordered systems as due to either localization or interaction effects. Localization theories[7–9] predict a logarithmic correction to the drude conductivity in a 2D disordered systems and

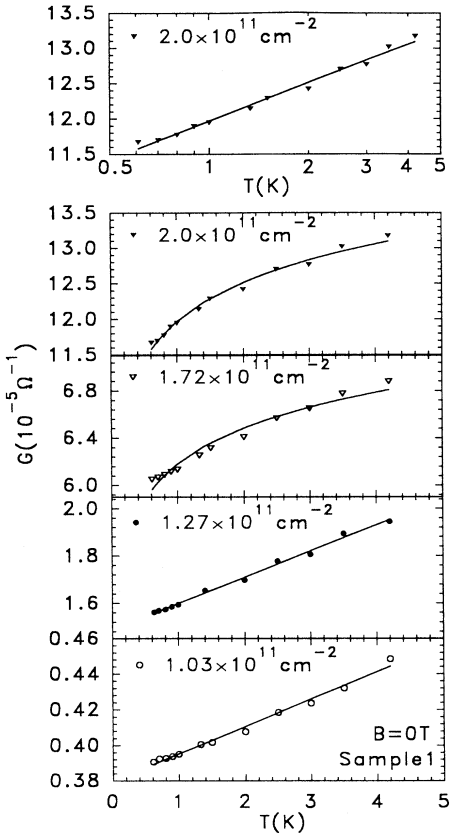

FIG. 5. The two types of temperature dependence of the conductance seen at high and low electron densities. The data are for sample 1. The conductance at 2.0×10^{11} cm^{-2} is drawn as a function of both $\ln T$ and T to demonstrate the $\ln T$ dependence at higher carrier density. The solid lines show the results of a least-square fitting to a simple linear T (lowest two traces) or $\ln T$ dependence (upper three traces).

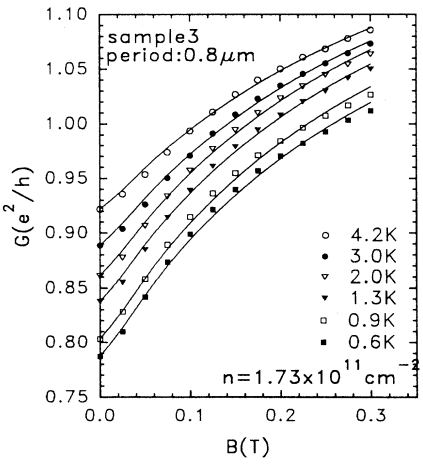

FIG. 4. Magnetoconductance as a function of B at six fixed temperatures at a carrier density of 1.73×10^{11} cm^{-2} measured on sample 3. Symbols are the measured results and the solid curves are calculated by Eq. (1) in Sec. IV with $K_1=1/9.5$ and $K_2=5/24$ for specular reflection (see text for details).

a $T^{-p/2}$ dependence for 1D, arising from a single electron scattered in a random impurity potential in the weak-field limit $\omega_c\tau_e \ll 1$, where $\omega_c=m^*/eB$ is the cyclotron frequency and τ_e is the elastic collision time with impurities. This effect is suppressed when $B \geq B_1 = \hbar/4eD\tau_e$, where D is the electron-diffusion coefficient. B_1 is typically around 0.1 T.[10] Electron-electron interaction theories also predict a logarithmic correction to the conductivity in 2D disordered systems, which is due to the enhanced Coulomb interaction between diffusively moving electrons[11,12] even in the regime of $\omega_c\tau_e \gg 1$.[13,14] The NMR due to this interaction, which is proportional to B^2 (Refs. 13 and 15) in both 1D and 2D systems, can be observed up to fields of $B \leq B2 = k_B T/g\mu_B$,[16–18] giving a parabolic curve. For GaAs in our samples, B_2 is estimated to be of order 1.5 T for the temperature range of interest. The two theories have been widely used to fit experimental data.[10–24]

However, the data presented above show a number of important differences from that seen in conventional disordered 2D systems, which makes the use of the con-

ventional theories inappropriate. Notably: (1) both the field range (in excess of 1 T) and the magnitude of the change in conductance (over 50% in some cases) are much larger than usual; (2) the low-field limit of the NMR is linear in B, in comparison with the parabolic behavior that is normally seen; (3) the NMR is strongly pattern dependent, mostly disappearing when the density is high and the patterning is screened out.

We therefore look to an explanation based on the presence of the antidot lattice.

We imagine the antidot lattice as the following. Each reservoir, in which the electron concentration is higher than in necks,[1] can be thought as a 2D electron gas (2DEG) with high mobility similar to the material before being patterned. The saddle-shaped potential between two adjacent implanted spots behaves as a constriction to the electrons with a width W_n and length l_n. The width W_n was estimated by letting $W_n = 2R_c(B)$, where $R_c(B)$ is the cyclotron radius at the magnetic field where the first strong SdH oscillation minima appear in the trace, which means the sample is in a 2D transport regime where the cyclotron radius is smaller than the half of the constriction width. Before putting electrons in the samples, the energy bottom of each neck should be the coincident point of the two equipotential lines from two adjacent depletion centers. We assumed that the screening distorts the equipotential circles in the neck region when the electrons populate the necks, leading to a W_n separation between two equipotential lines. By this geometrical relation we estimated l_n as $l_n \simeq \sqrt{2W_n d}$. These two parameters are also listed in Table I. For the electron elastic-scattering time τ_e in the necks, we approximate it as the same as that in the reservoirs. Physically, this corresponds to the assumption that the patterning process only caused periodical potentials in the 2D junction and no additional disorder scattering exists. Both the estimated τ_e and the mean free path of electrons l_e ($l_e = v_F \tau_e$, where v_F is the Fermi velocity) are listed in Table II for one sample using the measured carrier density and $\mu_e \propto (n_e)^{1.5}$ and the unpatterned mobility. We found, first of all, $l_e \gg W_n$, i.e., the electrons in the constrictions move ballistically from one side wall to the other and then are scattered by the boundary. The theory of weak localization in one-dimensional disordered systems[25] (AA theory) is not applicable in our case, since it is valid only if $l_e \ll W_n$. Second, as we will see below, $l_\phi \gg W_n$ holds for all our samples at the temperatures and the concentrations of interest, implying each constriction is a one-dimensional system in low fields just like that in a point contact.[20,26,27] Neglecting the resistance in each reservoir and assuming the net current in the transverse direction is zero, the patterned 2DEG can be thought as an array of one-dimensional point contacts in series and parallel connection. The number of the contacts is L/d and W/d in the two directions, respectively. Here L, W, and d are the length, the width of a 2DEG, and the pattern period, respectively.

Having set up such a physical picture, we found that the magnetoconductance properties of our samples should be described by the theory of one-dimensional weak localization modified by boundary scattering that was first studied for diffuse surface scattering by Dugaev and Khmelnitskii (DK) (Ref. 28) in the pure metal regime ($l_e \gg W$) in the weak and strong magnetic field limits and then extended by van Houghton *et al.*[29] to the crossover between the regimes of $l_e \ll W$ (AA theory) and $l_e \gg W$ (DK theory) in a narrow channel and a thin film including specular boundary scattering.

The theoretical expression for the magnetoconductance, $G(B)$ in such a one-dimensional channel, using a semiclassical approach ($\lambda_F \ll W_n$) under the diffusion approximation ($l_e < l_n$) can be described as follows:[29]

$$G(B) = G(0) - \frac{e^2}{\pi\hbar}\frac{\sqrt{D}}{l_n}\left[\left[\frac{1}{\tau_\phi}+\frac{1}{\tau_B}\right]^{-1/2} - \left[\frac{1}{\tau_\phi}+\frac{1}{\tau_B}+\frac{1}{\tau_e}\right]^{-1/2} - \left[\frac{1}{\tau_\phi}\right]^{-1/2} + \left[\frac{1}{\tau_\phi}+\frac{1}{\tau_e}\right]^{-1/2}\right], \quad (1)$$

where τ_ϕ is the phase-coherent time depending on temperature, D is the diffusion coefficient that simplifies to $D = (v_F W_n/\pi)\ln(l_e/W_n)$ in the limit $l_e/W \to \infty$, l_n is the length of each constriction, and τ_B is the phase-relaxation time

$$\tau_B = \frac{l_c^4}{K_1 W_n^3 v_F} + \frac{l_c^2 \tau_e}{K_2 W_n^2}, \quad (2)$$

where W_n is the width of each constriction, v_F is the Fermi velocity, and $l_c = \sqrt{\hbar/eB}$ is the magnetic length. K_1 and K_2 are two coefficients, depending on the scattering mechanism, with theoretical values of $K_1 = 1/9.5$ and

TABLE II. The characteristic parameters of the 2D array of point contacts.

n (cm^{-2})	τ_e (10^{-12} s)	l_e (μm)	B (10^{11}/s)	A (10^9 s/K)	A_{cal} (10^9 s/K)
1.03×10^{11}	3.93	0.64	2.25	6.93	9.17
1.27×10^{11}	5.38	1.08	0.69	4.29	6.35
1.37×10^{11}	6.03	1.29	0.84	4.50	5.52
1.72×10^{11}	8.48	2.29	0.30	2.48	3.59
2.0×10^{11}	10.6	3.35	0.19	2.00	2.68

$K_2=5/24$ for specular scattering, and $K_1=1/4\pi$ and $K_2=1/3$ for diffuse scattering.

Fixing the constants K_1 and K_2 and the estimated parameters for W_n and τ_e, we fitted the theory to our measured magnetoconductance by least squares using the phase-coherent time τ_ϕ as a fitting parameter. Figure 4 shows one of the fitting results for the magnetoconductance from sample 3 at 1.73×10^{11} cm^{-2} and Fig. 6 shows the fitting results for the phase-breaking rate $1/\tau_\phi$ as a function of temperature from sample 4. The smallest τ_ϕ at 4.2 K for all the samples is 3.75×10^{-12} sec. So the shortest phase-coherent length l_ϕ is calculated by $\sqrt{D\tau_\phi}$ to be 0.2 μm, which is much bigger than the width W_n. The fitting results can be summarized as follows. First, the fitting is good when values were taken for $K_1=1/9.5$ and $K_2=5/24$, which is consistent with a specular boundary-scattering mechanism for the electrons. Second, as shown in Fig. 4, good agreement was found up to 0.3 T at lower concentrations and 0.2 T at higher values. Above this field, disagreements begin due to the onset of SdH oscillations and the electron trajectory curves too much for this theory to be valid. The conducting channels became wider at higher densities owing to screening, so that the theory is only applicable in weaker fields. Third, the plot (Fig. 6) of the phase-breaking rate, which is the inverse of τ_ϕ, shows a linear increase as a function of temperature for all densities, which will be discussed in the following section. The same theory can be used to describe the conductances at both lower and higher concentrations and generates a linear dependence of the phase-breaking rate, independent of whether the *conductance* is in a region that has either a linear T or $\ln T$ dependence.

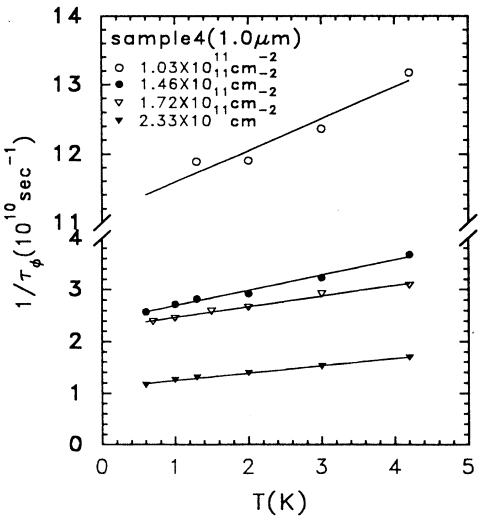

FIG. 6. The fitting results for the temperature dependence of the phase-breaking rate, $1/\tau_\phi$ from sample 4. The linear dependence of $1/\tau_\phi$ on temperatures occurring in all of the samples.

IV. DISCUSSIONS

From Tables I and II, the mean free path (l_e) is longer than the length of each constriction l_n which suggests that Eq. (1) is not applicable in our case because the diffuse approximation breaks down in this regime. However, we have two reasons to support our analysis in the above section. First of all, an electron experiences many boundary scattering events as it moves in a constriction from one end to the other, so that the actual path of the electron may be substantially longer than the physical length. Second, the boundary scattering happens not only in the constriction where the width is W_n, but also in the transition regions between the reservoirs and the one-dimensional constrictions, where the width is still smaller than or comparable to the mean free path in Table II. So the "effective" length could be much longer than the mean free path.

As mentioned above, Fig. 6 shows a linear increase of $1/\tau_\phi$ with temperature. In contrast, Choi, Tsui, and Palmateer[30] and Lakrimi[31] have found that the magnetoresistance of thin wires of GaAs/$Ga_{1-x}Al_xAs$ below B_c (defined by $l_c=W$) is independent of temperature when boundary scattering is dominant. In our case both the conductance and $1/\tau_\phi$ contain a term linear in temperature. We therefore conclude that there is an additional inelastic-scattering process present with a linear T dependence.

Since the phase coherence length l_ϕ estimated from τ_ϕ in Fig. 6 is longer than the constriction length for all of the data, we postulate that the majority of the additional scattering comes from the transition regions at either end of the 1D point contacts, where the width is comparable to the electron mean free path. The phase-breaking rate $1/\tau_\phi$ can then be expressed as

$$1/\tau_\phi=1/\tau_{\phi\mathrm{pc}}+1/\tau_{\phi\mathrm{tr}}\ , \tag{3}$$

where $1/\tau_{\phi\mathrm{pc}}$ is independent of temperature,[32] being proportional to the 1D boundary roughness scattering rate and the subscript pc denotes the point contacts. For the second term the subscript tr denotes the transitional region. There could be many sorts of inelastic-scattering mechanism. We have calculated the scattering rate of acoustic phonons with electrons which is proportional to T.[33,34] This rate is on the order of 10^8 (sec^{-1}), about one order of magnitude smaller than that in our data. For electron-electron scattering, the scattering rate is

$$1/\tau_{\phi 2\mathrm{D}}=\frac{\pi}{2}\frac{(k_BT)^2}{\hbar E_F}\ln\left[\frac{E_F}{k_BT}\right] \tag{4}$$

when $T>h/(k_B\tau_e)$ (Refs. 35 and 36) and

$$1/\tau_{\phi 2\mathrm{D}}=\frac{k_BT}{2E_F\tau_e}\ln\left[\frac{E_F\tau_e}{\hbar}\right] \tag{5}$$

when $T<h/(k_B\tau_e)$ (Refs. 35–37). In this work $h/(k_B\tau_e)$ is estimated at from 4.1 to 7 K, so the second formula is applicable in our case. We ascribe the second term of Eq. (3) to the electron-electron scattering in the transitional regions. Therefore, we have

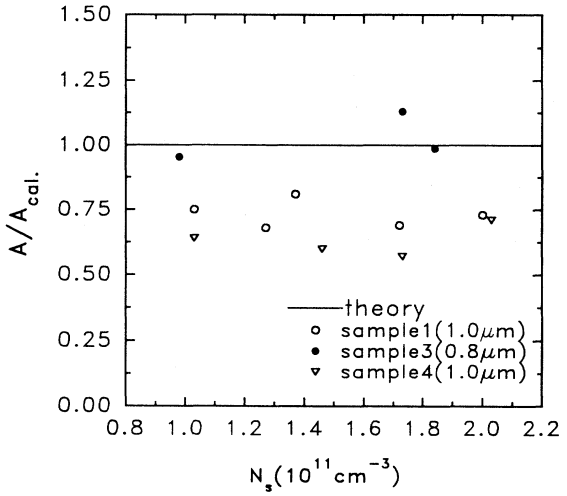

FIG. 7. The ratio of the fitted (A) to the calculated ($A_{\rm cal}$) linear temperature coefficient of the phase-breaking rate in sample 1 (○), sample 3 (●), and sample 4 (▽).

$$1/\tau_\phi = B + \frac{k_B T}{2E_F\tau_e}\ln\left[\frac{E_F\tau_e}{\hbar}\right] = AT + B \ , \qquad (6)$$

where B is a constant standing for the temperature-independent (boundary) scattering rate. By fitting a linear function of temperature to the measured curves in Fig. 6 (symbols), we obtained the slope A and the intercept B of the straight lines in Table II. The values of $A_{\rm cal}$ in the table are the calculated coefficients of the linear T term in Eq. (6) which are very close to the measured ones, the slopes of $1/\tau_\phi$ vs T in Fig. 6.

The excellent agreement can be seen in Fig. 7, which shows the ratio of A to $A_{\rm cal}$ for three different samples. In general, the measured values are a little below the calculated ones, as would be expected, since only a part of the mean free path will be within the transition regions.

In general the boundary scattering rate increases rapidly for the lower-density, more strongly modulated results, as would be expected qualitatively; however, no detailed theory of this yet exists with which to make a quantitative comparison.

Finally it should be remarked that although we are in the regime $l_e \geq l_n$, W_n, we would not expect to observe any conductance quantization in our structures, since we are making an ensemble average of $> 10^4$ point contacts. Thus, any small fluctuations in width or potential height will act to smear out the quantization. It is only when high magnetic fields are applied, as in paper I[1] that quantization can occur due to the much larger energy scale of the Landau levels.

V. CONCLUSIONS

We have demonstrated that a characteristic feature of an antidot lattice, acting as an array of point contacts, is a strong negative magnetoresistance. This is also found to be quite strongly temperature dependent, giving rise to a linear temperature dependence of the conductivity for strong patterning. Detailed analysis shows that the data can be fitted by a combination of boundary scattering in the point-contact regions and electron-electron scattering in the transition regions to the electron reservoirs. For more weakly modulated structures the same scattering mechanisms and analysis lead to a $\ln T$ contribution to the conductivity.

ACKNOWLEDGMENT

We acknowledge financial support from S.E.R.C. (U.K.).

[1]G. M. Sundaram *et al.*, preceding paper, Phys. Rev. B **47**, 7348 (1993).
[2]K. Ensslin and P. M. Detroff, Phys. Rev. B **41**, 12 307 (1990).
[3]T. P. Smith III, K. Y. Lee, C. M. Knoedler, J. M. Hong, and D. P. Kern, Phys. Rev. B **38**, 2172 (1988).
[4]K. Ismail, T. P. Smith III, W. T. Masselink, and H. I. Smith, Appl. Phys. Lett. **55**, 2766 (1989).
[5]E. H. Lindfield, D. A. Ritchie, G. A. C. Jones, J. E. F. Frost, and D. C. Peacock, Semicond. Sci. Technol. **5**, 385 (1990).
[6]Firoz Nasir, Ph.D. thesis, Clarendon Laboratory, Oxford University, 1986.
[7]P. W. Anderson, Phys. Rev. **109**, 1492 (1958).
[8]E. Abrahams, P. W. Anderson, D. C. Licciardello, and T. V. Ramakrishnan, Phys. Rev. Lett. **42**, 673 (1979).
[9]P. A. Lee, Rev. Mod. Phys. **57**, 287 (1985).
[10]B. J. F. Lin, M. A. Paalanen, A. C. Gossard, and D. C. Tsui, Phys. Rev. B **29**, 927 (1984).
[11]B. L. Altshuler, A. G. Aronov, and P. A. Lee, Phys. Rev. Lett. **44**, 1288 (1980).
[12]H. Fukuyama, J. Phys. Soc. Jpn. **48**, 2169 (1980).
[13]A. Houghton, J. R. Senna, and S. C. Ying, Phys. Rev. B **25**, 2196 (1982); **25**, 6468 (1982).
[14]S. M. Girvin, M. Jonson, and P. A. Lee, Phys. Rev. B **26**, 1651 (1982).
[15]B. L. Altshuler, D. Khmel'nitzkii, A. I. Larkin, and P. A. Lee, Phys. Rev. B **22**, 5142 (1980).
[16]Y. Isawa and H. Fukuyama, J. Phys. Soc. Jpn. **53**, 1415 (1983).
[17]B. L. Altshuler and A. G. Aronov, Solid State Commun. **46**, 429 (1983).
[18]C. Castellani, C. Di Castro, P. A. Lee, and M. Ma, Phys. Rev. B **30**, 527 (1984).
[19]M. J. Uren, R. A. Davies, M. Kaveh, and M. Pepper, J. Phys. C **14**, 5737 (1981).
[20]K. K. Choi, D. C. Tsui, and S. C. Palmateer, Phys. Rev. B **32**, 5540 (1985).
[21]M. A. Paalanen, D. C. Tsui, and J. C. M. Hwang, Phys. Rev. Lett. **51**, 2226 (1983).
[22]T. J. Thornton, M. Pepper, H. Ahmed, D. Andrews, and G. J. Davies, Phys. Rev. Lett. **56**, 1198 (1986).
[23]R. G. Wheeler, Phys. Rev. B **24**, 4645 (1981).
[24]M. J. Uren, R. A. Davies, M. Kaveh, and M. Pepper, J. Phys. C **14**, L395 (1981).
[25]B. L. Altshuler and A. G. Aronov, Pis'ma Zh. Eksp. Teor. Fiz. **33**, 515 (1981) [JETP Lett. **33**, 499 (1981)].

[26]B. J. van Wees, *et al.*, Phys. Rev. B **38**, 3625 (1988).
[27]B. J. van Wees, *et al.*, Phys. Rev. Lett. **60**, 848 (1988).
[28]V. K. Dugaev and D. E. Khmel'nitskii, Zh. Eksp. Teor. Fiz. **86**, 1784 (1984) [Sov. Phys. JETP **59**, 1038 (1984)].
[29]H. van Houten, C. W. J. Beenakker, B. J. van Wees, and J. E. Mooij, Surf. Sci. **196**, 144 (1988).
[30]P. G. de Gennes and M. Tinkham, Physics (NY) **1**, 107 (1964).
[31]M. Lakrimi, Ph.D. thesis, Sussex University, 1987.
[32]It has been shown that surface roughness scattering is independent of temperature for the 2DEG in a silicon inversion layer. A. Hartstein, A. B. Fowler, and M. Albert, Surf. Sci. **98**, 181 (1980).
[33]F. Stern, Phys. Rev. B **5**, 4891 (1972).
[34]P. Streda, J. Kucera, and A. H. MacDonald, Phys. Rev. Lett. **59**, 1973 (1987).
[35]B. L. Altshuler, A. H. Aronov, and D. E. Khmelnitsky, J. Phys. C **15**, 7367 (1982).
[36]H. Fukuyama, J. Phys. Soc. Jpn. **53**, 3299 (1984).
[37]H. Fukuyama, and E. Abrahams, Phys. Rev. B **27**, 5976 (1983).